PHYSICAL REVIEW B **87**, 115425 (2013)

Scattering of surface electrons by isolated steps versus periodic step arrays

J. E. Ortega,[1,2,3] J. Lobo-Checa,[2] G. Peschel,[4,5] S. Schirone,[4,6] Z. M. Abd El-Fattah,[3] M. Matena,[3] F. Schiller,[2] P. Borghetti,[3] P. Gambardella,[4,7] and A. Mugarza[4]

[1]*Universidad del País Vasco, Departmento Física Aplicada I, E-20018 San Sebastián, Spain*
[2]*Centro de Física de Materiales CSIC/UPV-EHU-Materials Physics Center, Manuel Lardizabal 5, E-20018 San Sebastián, Spain*
[3]*Donostia International Physics Center, Paseo Manuel Lardizabal 4, E-20018 Donostia-San Sebastián, Spain*
[4]*Catalan Institute of Nanotechnology (ICN), UAB Campus, E-08193 Bellaterra, Spain*
[5]*Institut für Experimentalphysik, Freie Universität Berlin, Arnimallee 14, 14195 Berlin, Germany*
[6]*Dipartimento di Fisica, Sapienza Università di Roma, Piazzale Aldo Moro, 5, I-00185 Roma, Italy*
[7]*Institució Catalana de Recerca i Estudis Avancats (ICREA), E-08193 Barcelona, Spain*

(Received 30 January 2013; published 20 March 2013)

We investigate the scattering of electrons belonging to Shockley states of (111)-oriented noble metal surfaces using angle-resolved photoemission (ARPES) and scanning tunneling microscopy (STM). Both ARPES and STM indicate that monatomic steps on a noble metal surface may act either as strongly repulsive or highly transmissive barriers for surface electrons, depending on the coherence of the step lattice, and irrespectively of the average step spacing. By measuring curved crystal surfaces with terrace length ranging from 30 to 180 Å, we show that vicinal surfaces of Au and Ag with periodic step arrays exhibit a remarkable wave function coherence beyond 100 Å step spacings, well beyond the Fermi wavelength limit and independently of the projection of the bulk band gap on the vicinal plane. In contrast, the analysis of transmission resonances investigated by STM shows that a pair of isolated parallel steps defining a 58 Å wide terrace confines and decouples the surface state of the small terrace from that of the (111) surface. We conclude that the formation of laterally confined quantum well states in vicinal surfaces as opposed to propagating superlattice states depends on the loss of coherence driven by imperfection in the superlattice order.

DOI: 10.1103/PhysRevB.87.115425 PACS number(s): 79.60.Jv, 73.20.At, 73.22.−f

I. INTRODUCTION

Scanning tunneling microscopy (STM) has made widely popular the scattering of electrons at surface defects, such as atomic and molecular adsorbates and monatomic steps.[1–9] The importance of such interference patterns goes beyond their aesthetic appeal since they actually mirror fundamental properties of solid crystals related to electron transport and quantum confinement. For example, the inelastic lifetime and quantum coherence of a scattered electron, which is derived from the decay length of standing waves away from surface steps.[7] And the contrary case, i.e., the lack of back-reflected waves near a step, which straightforwardly proves the time-reversal spin-orbit asymmetry of surface bands in topological insulators.[10,11]

The absence of chiral spin textures in noble metal surfaces, such as Ag and Cu, makes them very attractive as reference systems for surface scattering phenomena. Based on the earliest analysis of STM interference patterns,[1,8] steps and metallic adsorbates at (111)-oriented surfaces are frequently assumed as canonical hard-wall potential barriers, on which surface electron waves undergo substantial reflection (R) and absorption (A) but negligible transmission (T). However, the nature of the step potential in a noble metal surface is more complex and fundamental questions remain open. First, the fact that, in contrast to the hard wall behavior observed in STM, angle-resolved photoemission (ARPES) experiments, performed in vicinal (111) noble metal surfaces, have repeatedly shown dispersing bands with clear signatures of weak repulsive scattering at steps, namely small size effects and narrow gaps at the Brillouin zone boundary.[12–15] This behavior is only compatible with a high transmission coefficient T across the step barrier. The weak scattering in the step array of the vicinal surface demonstrated in ARPES is consistent, though, with the only STM study of the Shockley state performed on a vicinal plane. In fact, Hansmann *et al*. analyzed the standing wave patterns around a defect in Cu(554),[16] and determined a surface band energy that completely agrees with ARPES results.[14] Altogether, ARPES and STM studies agree with the double scenario sketched in Fig. 1. Incoherent, random steps act as quasi-hard-wall potentials that confine electrons inside (111) terraces, whereas periodically arranged steps behave as transparent barriers, which allow coherent coupling from terrace to terrace, and hence Bloch states of a step superlattice. But, why does the step barrier strength change that much when going from a defectlike, random step, to the staircase of the vicinal surface?

The different scattering behavior of surface steps as single entities or as periodic arrays is surely connected with the so-called wave function modulation plane.[17] In reality a true surface state is defined by the crystal plane of the surface. In a vicinal surface, such plane is coherently determined by step edge atoms that define a step superlattice. The surface state becomes a Bloch state of the superlattice, with its two-dimensional, dispersing component of the wave function being modulated by the steps of the average (vicinal) surface plane, as sketched in Fig. 1(a). If the surface state loses coherence, it gets confined within a single terrace, and the wave function component perpendicular to the step becomes a quantum well oriented along the (111) terrace, as represented in Fig. 1(b). The second question that arises is whether a critical step spacing exists in a superlattice, for which coherence is lost,[12] or it is simply disorder in the step array that causes the lack of coherence and the confinement of the surface state.[13]

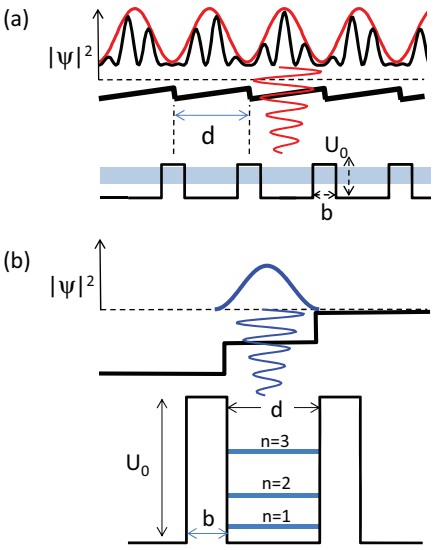

FIG. 1. (Color online) Side-view sketch of (a) step-modulated superlattice states for a 1D periodic potential in a vicinal surface with lattice constant d and weak U_0b barriers at step edges. (b) Surface quantum well states confined by effectively stronger U_0b potentials in (111) terraces. As depicted in both panels, the modulation plane in each case determines the direction along which the wave function decays towards the bulk crystal, i.e., perpendicular to the average surface plane in (a) and perpendicular to the (111) terrace in (b). Such decaying part of the wave function is essential to understand the diffraction plot of Figs. 3 and 4.

In this paper we revisit these concepts combining STM and ARPES experiments in decoupled and coherent step arrays, respectively. By examining the same step spacing range, we confirm the distinct scattering scenario depicted in Fig. 1, but discard the existence of any critical superlattice constant. In ARPES we make use of state-of-the-art curved surfaces to accurately determine the surface state wave function modulation plane for periodic step arrays with large spacing. We observe coherent superlattice states beyond $d > 100$ Å periodicity, in the limits of ARPES resolution. In STM, following the method of Seo *et al.*,[11] we carefully check for the existence of transmission resonances out of an isolated (111) terrace, defined by two parallel steps separated by $d < 100$ Å. We observe possible traces of leakage out of such narrow terrace, but close to the limits of the STM detection, i.e., we confirm that individual steps act as quasi-hard-wall potentials for (111) surface states.

II. EXPERIMENTAL METHODS

ARPES measurements were carried out at the PGM beamline of the Synchrotron Radiation Center (SRC) in Stoughton (Wisconsin). We used a hemispherical Scienta SES200 analyzer with energy and angular resolution set to ~30 meV and 0.1°, respectively, and p-polarized light with the polarization plane parallel to surface steps. Au and Ag single crystals are cut and polished defining a $\alpha = \pm 15^\circ$ cylindrical surface (11.6 mm radius) around the [111] direction ($\alpha = 0$). Such cylindrical surfaces are prepared in vacuum following standard ion sputtering plus annealing cycles. The 100 μm diameter photon beam is scanned on top, allowing us to select the crystal orientation (or miscut angle α) with an effective $\Delta\alpha \sim 0.25^\circ$ spread of the beam. The samples were mounted with the $[11\bar{2}]$ crystal direction running parallel to the analyzer entrance slit, such that the 1D step superlattice band dispersion could be directly imaged in the channelplate detector of the analyzer. For linefit analysis, channelplate images were decomposed in single energy dispersion curves (EDC) for each of the 127 channels. Peak fits were carried out using distinct Lorentzian lines for the pair of umklapp surface states (when visible), convoluted by Gaussians to account for temperature and experimental resolution. The series of fits determined peak energy, width, and intensity at all photon energies.

STM experiments were performed at 5 K, using isolated terraces on the surface of a Ag(111) single crystal. Conductance (dI/dV) spectra were obtained with the lock-in technique, using a bias voltage modulation of frequency 3 kHz and amplitude 3 mV_{rms}. The energy-dependent modulation of the dI/dV signal originating from the electronic structure of the tip was effectively removed by subtracting a background spectrum to the data.[18] The latter was acquired at least 600 Å away from any step or impurity in order to avoid any modulation resulting from scattering. The spatial modulation of the quantum well states (QWS) was deconvoluted from intensity variations related to changes in tip-sample distance by subtracting the otherwise featureless pre-edge intensity below the onset of the surface state.

III. SUPERLATTICE STATES MODULATED ON THE VICINAL PLANE: PHOTON-ENERGY-DEPENDENT ARPES

Figure 2 illustrates the photon-energy dependence of surface bands measured in step arrays of Au and Ag with relatively large step spacing. Data have been taken using curved crystals at -1.9° and 3.6° miscuts, which correspond to the Au(13 14 14) and Ag(778) surface planes, with $d = 71$ Å and $d = 38$ Å lattice constants, respectively. Both surfaces exhibit a two-dimensional surface band with the characteristic signatures of scattering by the step superlattice, namely the upwards shift of the band with respect to the (111) surface, analyzed in detail in Ref. 14, and the presence of $2\pi/d$ superlattice folding. There is a significant superlattice zone-edge gapping, although it is blurred by the inherent size distribution broadening of the step array. Superlattice gaps can be made visible in second derivative intensity plots at low photon energies.[19]

The strong photon-energy-dependent cross section shown in Fig. 2 is related to the nature of the superlattice state wave function, and it is better explained through Fig. 3. Notice that the wave vector axis in Fig. 2 is referred to the respective local surface plane, i.e., the vicinal surface, where umklapps perfectly align at π/d and $3\pi/d$ zone-boundary edges. The umklapp alignment at zone-boundary edges is the important feature that proves that superlattice states are step-modulated, as described in Fig. 1(a), and hence that the step barrier potential needs to be relatively weak. The latter can be determined from the fit to the gapped superlattice band structure,[13,19] although it can be estimated in a more straightforward way from the surface band shift with respect to the (111) direction and using a 1D Kronig-Penney model.[14]

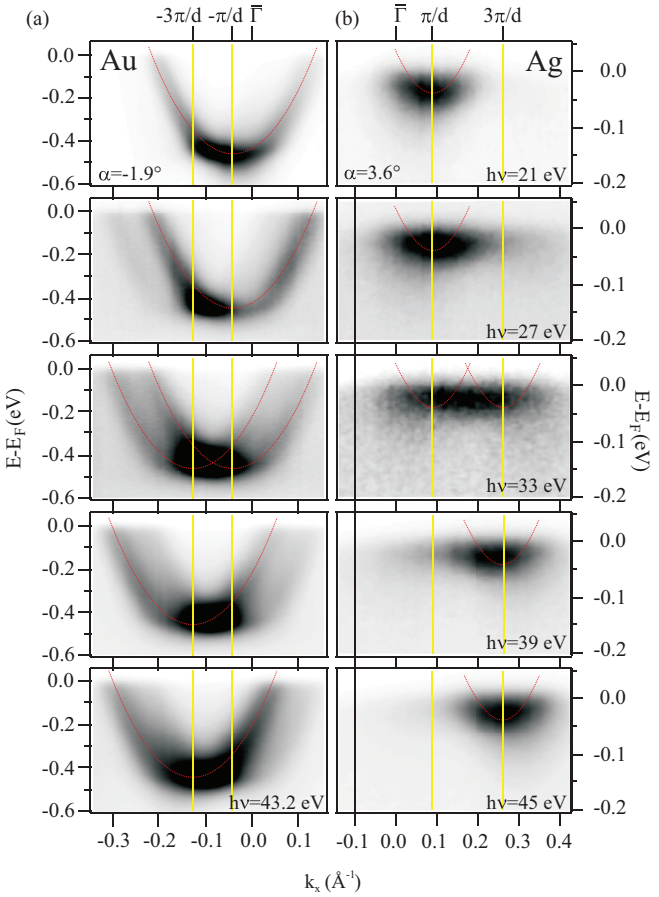

FIG. 2. (Color online) Photon-energy-dependent band dispersions for (a) Au and (b) Ag step lattices, respectively measured at -1.9° and 3.6° from the (111) surface in a curved crystal. Vertical solid lines mark zone-boundary edges of the step superlattice. Umklapp bands align at zone-boundary edges, as expected for the step-modulated surface state shown in Fig. 1(a). By increasing the photon energy, the intensity jumps from first order (π/d) to second order ($3\pi/d$) rods, as in low energy electron diffraction from vicinal surfaces.[20]

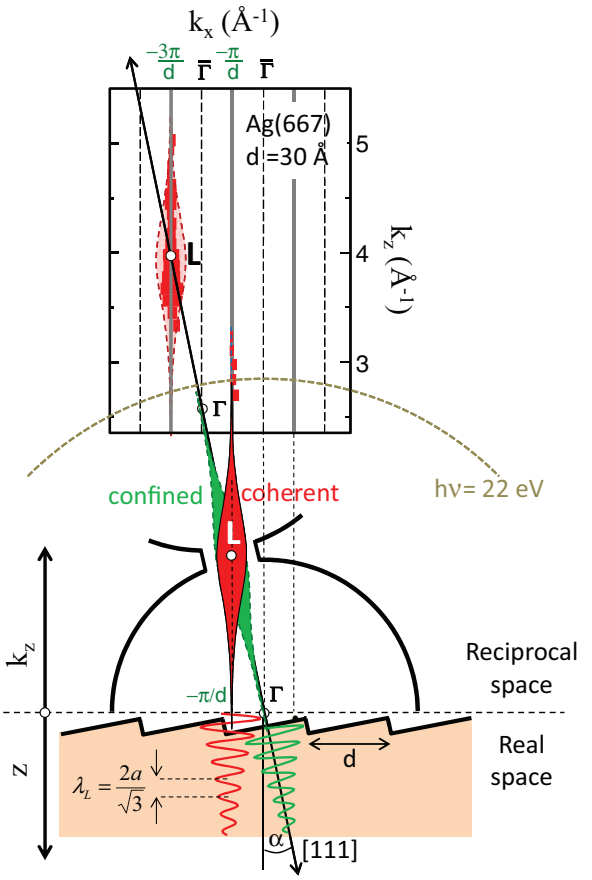

FIG. 3. (Color online) Analysis of the Fourier components of the surface states through diffraction plots. The bottom panel sketches the exponential decay of the surface state wave function (wavelength λ_L) towards the bulk (z direction) in the two different cases of Fig. 1, namely coherent surface states of the 2D step lattice plane (red wave) and quantum wells, confined in (111) terraces (green wave). Such exponential attenuation gives rise to the complete broadening in reciprocal space in the corresponding bulk directions, with maximum weight at the L point (wave vector $k_L = 2\pi/\lambda_L$). For coherent waves, the spectrum is broadened along the k_z direction (red cigar), for confined states Fourier components spread along the [111] direction (green cigar). The coherent, k_z broadening is experimentally demonstrated in the top panel. Here we represent (red rectangles) the photoemission intensity of the surface state band minimum as a function of k_x and k_z. The width of each rectangle represents the peak intensity, such that the set of data mirrors the red-cigar-shaped Fourier composition of the bottom panel. Two umklapp rods are observed, with the spacing corresponding to coherent superlattice states of the 2D step array.

In sparsely separated step lattices, the latter procedure gives $U_0 b = 2.0$ eV Å and $U_0 b = 0.6$ eV Å for Au and Ag, respectively, where U_0 is the height and b the width of a square potential barrier. Finally, in Fig. 2 the observation of well-separated umklapps is not only restricted to the intermediate photon-energy range, but also to the ability to resolve the split bands. The latter is limited in Ag due to the close proximity of the Fermi edge and its broader terrace-width distribution.[14]

The superlattice state in Fig. 2 is the well-known 2D Shockley-like surface state that undergoes Bloch scattering by the step lattice.[14,21] Its physical nature can be probed by ARPES, and rationalized through the so-called diffraction plot of Fig. 3. The name comes from the resemblance with the low energy electron diffraction analysis of vicinal surfaces.[20] Figure 3 displays the same (x,z) plane of Fig. 1, at which superlattice states are defined by, first, Bloch waves in the perpendicular direction of the steps (x), and second, the exponentially decaying tail in the orthogonal bulk direction (z). The decaying tails of the two types of surface states, i.e., coherent 2D states and confined 1D states are shown in the bottom panel of Fig. 3. The corresponding reciprocal space description of the Shockley electron is sketched right above this panel. The thick curved line represents any constant energy surface of the bulk s,p band close to E_F in the k_x-k_z plane, with its characteristic neck at the L symmetry point. Superlattice Bloch waves in the x direction transform in $2\pi/d$ umklapps along k_x, whereas the oscillatory damping in the bulk direction results in a complete k_z broadening centered around the fundamental frequency ($k_L = \sqrt{3}\pi/a$, where a is

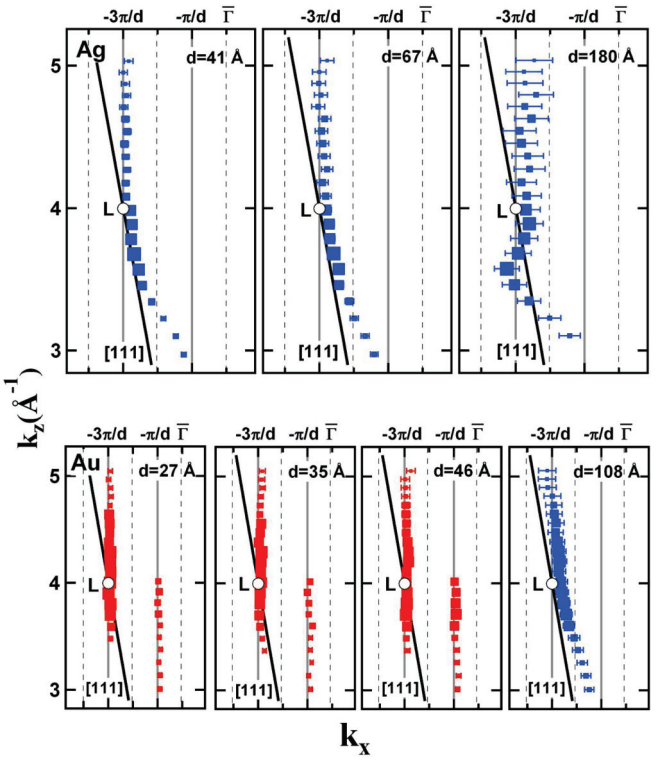

FIG. 4. (Color online) Diffraction plots for Ag (top) and Au (bottom) step arrays. Step lattice constants are indicated in the figures. Red data belong to lattices that exhibit split bands, where band minima (k_x in the figure) are determined by parabolic fitting. $3\pi/d$ and the π/d vertical rods with peaking intensity near the L point are probed, demonstrating superlattice Bloch scattering. Blue data points correspond to lattices where a double band cannot be resolved, and k_x data are determined from intensity maxima. In this case, split rods are not perfectly resolved around at intermediate energies Γ, although alignment along the [111] direction (solid black lines) never occurs.

the bulk lattice constant) at the L-point neck (gap). Thus, the intensity distribution along k_z can be represented by the width of the cigar-shaped rod in Fig. 3, with maximum weight at the L neck. The Fourier space representation of the modulation plane is beautifully tested by ARPES, as shown on the top panel of Fig. 3. Rectangular red data correspond to the surface state band bottom measured for a $d = 30$ Å step array in the curved Ag crystal at different photon energies (from 21 to 90 eV). The photon energy ($h\nu$) defines the constant energy curve (dashed curve) reachable by the photoelectron and hence the k_x-k_z plane can be scanned by varying $h\nu$. The peak intensity is reflected in the width of the rectangles, which define the expected cigar shape. In reality the spectral distribution is not perfectly mirrored since it is affected by the complex photoemission process.[22] Nonetheless, the π/d and $3\pi/d$ vertical "diffraction" rods are clearly demonstrated, as well as the peaking intensity around L.

Using the framework of Fig. 3, in Fig. 4 we explore the limits of coherent superlattice Bloch scattering for Au and Ag step arrays. The diffraction plot analysis is extended to the smallest miscut that can be reliably probed in ARPES. Red and blue data points respectively refer to cases for which one can resolve two separate split bands, as in Fig. 2(a), or cases where such bands are not resolved, although their existence is clearly suggested, as in Fig. 2(b), $h\nu = 33$ eV. For the former we determine the two band minima by parabolic fit to the split bands, and for the latter we choose the k_x value at which the intensity is maximum. Both Ag and Au exhibit, within error bars, the same behavior observed in Fig. 3, namely two separate $(2n + 1)/2 \times \pi/d$ diffraction rods and the L-point peaking intensity. Au band data align vertically at $k_x = \pi/d$ and $3\pi/d$ zone-boundary edges for 27, 35, and 46 Å superlattice constants.[23] Vertical zone-boundary-edge alignment of surface bands is also observed in the 71 Å lattice of Fig. 2(a), but for the 108 Å superlattice one cannot resolve two separate π/d and $3\pi/d$ rods around the zone center $\overline{\Gamma}$ (or bulk Γ projection). This results in the apparent alignment of data points along the [111] direction at this energy range. A similar behavior is found for 42 and 67 Å lattices in Ag, i.e., a clear alignment at zone-boundary edges, but inability to resolve the splitting around the bulk Γ point. Nonetheless, a perfect alignment of the whole set of data points along the [111] direction, as expected for confined quantum wells (blue cigar in Fig. 3), is not observed.

The deviation of vertical zone-boundary-edge alignment toward the [111] direction, shown in Fig. 4 for Au and Ag step lattices with large spacing, was also observed in the early diffraction plots of vicinal Cu(111), and attributed to a switch in the modulation plane of the superlattice state.[17,21] Figure 4 suggests that this is just an apparent alignment at intermediate photon energies, when both split bands are detected but not resolved, which in turn depends on both the experimental accuracy and the quality of the step array. The latter may be worse in Cu(111), which shows structural instabilities.[14] A change in modulation plane can exist, but triggered by a loss of superlattice coherence, which results in an effective confinement within randomly decoupled terraces.[13] Only if the latter affects a sizable portion of the crystal could it also be detected with ARPES.[15] Interestingly, despite the higher step barrier potential measured for Au superlattices,[14] we observe in Figs. 3 and 4 the perfect alignment of the Au k_x-k_z data along the π/d and $3\pi/d$ umklapp lines. Au in fact exhibits the sharpest step lattices,[19] and hence it is the superlattice order and not the barrier potential itself, the key parameter, that determines coherent coupling through steps. Therefore, we conclude that in the limit of the ARPES ability to resolve superlattice diffraction, Ag and Au step lattices behave as coherent crystals that scatter Shockley-like $2\pi/d$ Bloch waves.

Figures 3 and 4 are the most straightforward proof that surface states in step arrays are 2D superlattice states, which in turn are only possible for partially transparent step barriers that allow coherent coupling. In the past, the question arose whether such coupling occurred for a sufficiently large step spacing d. Indeed, it was argued that surface states in step arrays undergo a transition at a critical $d \sim 17$ Å value,[12,17,24] such that they become effectively decoupled and confined within (111) terraces. For such transition two reasons were given. First, the appearance of lattice instabilities and disorder at the critical value of $d = \lambda_F/2 \sim 17$ Å.[13] Terrace-width instabilities are in fact observed in STM experiments on curved Cu crystals around $d = \lambda_F/2$.[14] And second, the closing of the bulk projected gap at $d \sim 11$–17 Å, which leads to the smooth transformation of the surface state into a surface resonance, and

its corresponding reduction of the sensitivity of electrons to the step barrier.[12] Figure 4 discards such critical transformation in the surface state, proving that coherent coupling dominates for step arrays up to $d \sim 100$ Å lattice constant, i.e., well beyond the critical $d = \lambda_F/2$ or the projected bulk-gap closing value in both Ag or Au vicinal surfaces.

IV. 1D QUANTUM WELL STATES ON ISOLATED (111) TERRACES: MEASURING LEAKAGE THROUGH STEPS WITH STM

Our study of the surface state dispersion along step superlattices suggests that disorder in the step array, although not linked to any critical phenomenon, may in fact be the determinant factor for the loss of coherence of the superlattice Bloch state and its consequent localization on individual terraces. The lack of coupling through disordered steps can be understood on grounds of the energy mismatch between electrons in adjacent terraces since the resonant conditions depend critically on terrace size.[25] A more critical test of the transmission of surface waves across steps can be performed by studying the limiting case where an isolated terrace containing QWS is surrounded by large terraces with a continuum density of states (DOS). Here, coupling between terraces is not forbidden by energy matching conditions and leaking QWS with finite transmission through steps could in principle be found even in the absence of an ordered step array. Such systems can be ideally explored using the local spectroscopic capability of the STM.

Quantum confinement on single Ag(111) terraces of similar and smaller size have previously been studied.[8,25] Yet, studying leakage out of an isolated terrace has proven to be a difficult task. The analysis of the energy and spatial distribution of the QWS within the Fabry-Perot interferometer model leads to an accurate determination of the reflection coefficient. However, this method is not appropriate to study transmission since the latter is only reflected in the phase of the QWS, which in the model depends on the correct definition of the step boundaries. Models based on fitting the DOS at a confining terrace by using a pair of complex square potential barriers also fail by giving inconsistently large transmission probabilities.[25] Recently, Seo *et al.* proposed a multiple electron scattering method to study transmission through steps in a more direct way, by measuring the intensity modulation of the continuum DOS of a large terrace adjacent to a small terrace exhibiting QWS.[11] The transmission probability between terraces resonate at energies of the QWS, which produces dips in the intensity of the Friedel oscillations at the large terrace at the resonating energies. By using this method we study the leakage out of isolated Ag(111) terraces of size $d < 100$ Å, range where vicinal surfaces clearly exhibit dispersing superlattice states.

Figure 5 shows an example of such study with an isolated terrace of $d = 57.5$ Å surrounded by two large terraces. We focus our study on the right terrace. With its size of 1220 Å much larger than the coherence length of the Shockley state,[7] we can consider it as a semi-infinite terrace with a single step, namely the one separating it from the smaller terrace on the left. dI/dV spectra acquired along the line indicated on the topographic image are plotted in color scale after properly normalizing it as described in Sec. II. Here

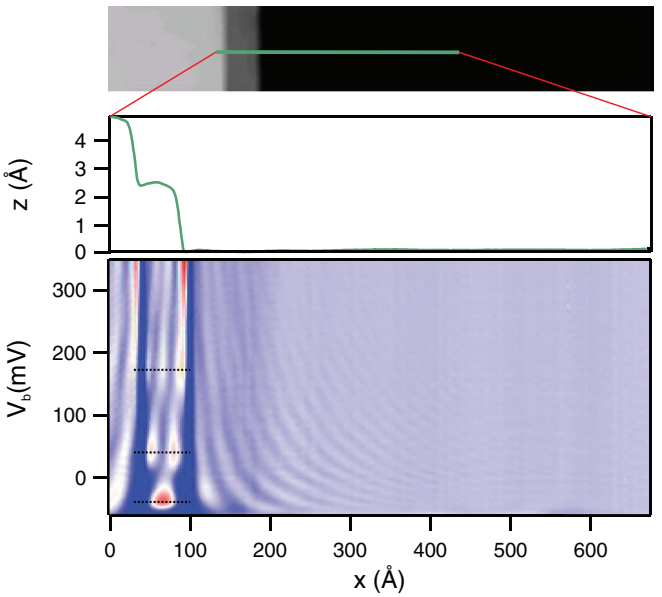

FIG. 5. (Color online) Standing wave patterns inside and outside an isolated terrace of $d = 57.5$ Å. The color plot corresponds to dI/dV data acquired along the line represented by the topographic profile on top. The spectra, obtained with setpoint values of $I = 0.43$ nA, $V_b = -100$ mV, has been normalized as indicated in Sec. II. Inside the terrace the coherent scattering at both steps produces nondispersing quantum well states (dashed lines) separated by energy gaps, whereas scattering at a single step in the neighboring larger terrace produce Friedel oscillations in the continuum of the surface state band.

we can easily differentiate the QWS of the small terrace from the Friedel oscillations of the large one: Coherent scattering at the two steps results in nondispersing, discrete electronic levels (dashed lines) separated by forbidden energy gaps in the small terrace, whereas in the large one scattering at a single step generates standing waves at the continuum of the surface DOS.

The spectra can also be presented by spatially averaging them on each terrace in the x direction (perpendicular to the steps), as displayed in Figs. 6(a) and 6(b) before and after the normalization, respectively. The spectra of the small terrace (blue) exhibits a strong modulation in energy arising from the quantum confinement. In contrast, the averaged spectra at the large terrace (red) is rather featureless. In fact, after subtracting the reference spectra, and hence any variation related to the electronic structure of the tip and the DOS of the infinite terrace, the normalized spectra become totally flat [see Fig. 6(b)]. The lack of any energy-dependent modulation in Ag(111) indicates that transmission through steps in this surface approaches zero at the level of resolution of our experiment.

Next we compare the energy of the QWS with that of an infinite quantum well, which are given by $E_N = E_0 + \hbar^2/2m^* \times (N\pi/d)^2$. We can do that without using any free parameter since we know the terrace size ($d = 57.5$ Å) from the topography, and the band bottom E_0 and effective mass m^* can be derived by fitting the experimental dispersion relation of Fig. 6(c) with that of the nearly free electron

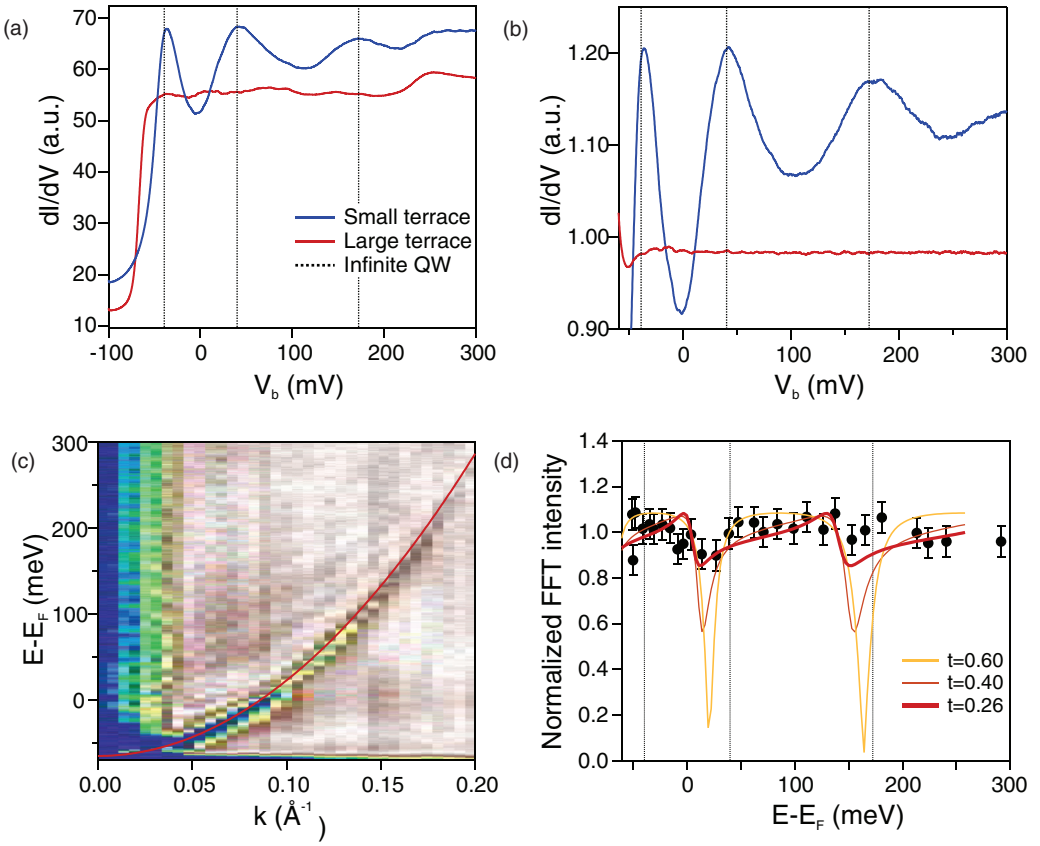

FIG. 6. (Color online) Analysis of the transmission through steps via the intensity modulation of Friedel oscillations. (a) dI/dV spectra spatially averaged over the small (blue) and large (red) terraces of Fig. 5. (b) Same as (a) after background subtraction. (c) Fourier transform of the spectra of the large terrace along the x direction. Under such transformation, the wavelength defined by the Friedel oscillations transforms as momentum, and the energy dispersion relation is derived. From the fit of the data with a parabola, the values of $E_0 = -66 \pm 2$ meV and $m^*/m_0 = 0.43 \pm 0.04$ are obtained. (d) Normalized intensity of the parabolic dispersion as a function of energy, after an exponential background substraction. Small dips appear at energies slightly bellow the $N = 2$ and $N = 3$ resonances, which may be viewed as traces of leakage out of the QW (see the text). The data is compared to the intensity modulation function of Ref. 11, for a reflection coefficient of $R = 0.8$, and using different values of transmission T. The three curves are shifted in energy by -42 meV. Vertical lines in (a), (b), and (d) represent the energies of an infinite 1D QW, using the values of E_0 and m^* obtained in (c).

$E = E_0 + \hbar^2/2m^*k^2$. The dispersion relation can be directly obtained by Fourier transforming the spectroscopic data of the large terrace of Fig. 5 along the x axis, which transforms the periodicity of Friedel oscillations at each energy in the corresponding wave vector k. From the parabolic fit to the band, we obtain $E_0 = -66 \pm 2$ meV and $m^*/m_0 = 0.43 \pm 0.04$, in close agreement with previous measurements.[6,26,27] By using these values we see how the peak energies of the QWS at the small terrace fits very well with the energy levels of the infinite quantum well [vertical lines in Figs. 6(a) and 6(b)], indicating again that transmission is negligible in this surface.

Finally, we check any possible quantum well leakage through the spectral weight variation along the dispersing band in Fig. 6(c). This leads to an energy-dependent curve that, after the subtraction of a smooth exponential background, can be fitted with an analytical function that depends on T, R, and A.[11] As in real space, the possible leakage effects should appear as an energy-dependent modulation, with dips at the energies of the QWS of the adjacent terrace. Such analysis is shown in Fig. 6(d), where we plot the spectral weight intensity variation along the band of Fig. 6(c), after subtraction of the exponential damping. We indeed observe a small dip at an energy slightly below the $N = 2$ resonance (arrow), and a much less defined one around the $N = 3$ QW energy. Although they fall at the limits of the experimental accuracy and appear slightly shifted to lower values as compared to the resonance energies, we may still consider such dips to obtain an upper estimate for the quantum well leakage, following the model of Ref. 11. For the sake of comparison, in Fig. 6(d) we plot the curve for $R = 0.8$ and different values of T. We note again that we have to shift the energy axis of the curves by -42 meV to account for the observed shift of the dip at $N = 2$. Although the possible interference from other scattering sources such as surface impurities have been carefully avoided, the mismatch between the energy of the dip and that of the QWS of contiguous terraces suggest that they may originate from the contribution of weak scatterers that cannot be easily detected from dI/dV maps, such as buried impurities. In any case, for a reflection coefficient $R = 0.6$–0.8 obtained by the Fabry-Perot model

in this energy range,[8] reasonable fits are obtained only for transmission probabilities $T^2 < 0.1$.

The upper estimate of $T^2 < 0.1$ for the transmission probability sets a limit to the hard-wall potential generally assumed for a noble metal surface.[1,8,11] However, this value is still too low compared with the high transmission required to explain the ARPES data. In particular, at the energy of the $N = 2$ resonance of Fig. 6, and assuming the weak $U_0 b \sim 0.6$ eV Å step barrier deduced for Ag steps in the 1D Kronig-Penney analysis of Ref. 14, it is straightforward to determine a transmission coefficient $T^2 \sim 0.78$ for step arrays.[12] One may be tempted to question the excessive simplicity of a 1D Kronig-Penney analysis based on the bare shift of the surface band with respect to the (111) surface state.[12,14] However, the Kronig-Penney model can be successfully used to fit the entire superlattice band structure in Au(788), where the quality of the step array allows a clear observation of dispersing bands and zone-boundary-edge minigaps.[19] On the other hand, since the probing depth in STM is limited to the outermost surface layer, one may appeal to a more complex Fourier composition of the surface state in the k_z-k_x plane in subsurface layers,[28] which would be dominant in ARPES measurements. Unfortunately, an accurate, first-principles calculation of surface states in vicinal planes with large step spacing is unfeasible yet. The reality is that isolated steps, which STM probes as defects in real space, possess very weak transmissivity, whereas Bloch waves formed in periodic arrays exhibit high transmission probability. Traces of the coexistence of 1D confined states and 2D coherent bands in real space have been found in STM conductance spectra performed on Cu(554).[16] Yet, the question remains why the barrier strength is different in each case.

V. CONCLUSION

The two systems studied in this work represent limiting cases in the correlation of electron scattering at monatomic steps of the Ag(111) surface. In high quality step superlattices, coherent coupling through steps result in highly transmissive barriers that allow the formation of 2D Bloch superlattice states even for step separations $d > 100$ Å, which are comparable to the intrinsic coherence length of the surface state at an infinite terrace.[7] Previously suggested terrace size-dependent transitions in the step potential barrier are discarded by both the fit of the energy shift with a single value for the barrier[14] and the observation of step-modulated superlattice states up to the largest step separation measurable by photoemission, which is well above the critical terrace sizes predicted in the past. We observe similar behavior for vicinal Ag(111) and Au(111) surfaces, where the potential barrier differs by as much as a factor of 4. Thus, we conclude that, although the magnitude of the step potential barrier could play a role, the determinant factor for the formation of QWS in vicinal surfaces observed in some cases is the loss of coherence driven by imperfections in the superlattice order. This is further demonstrated by studying the transmission in isolated terraces of similar $d < 100$ Å size. By using a method that directly addresses transmission resonances between confining (small) and semi-infinite (111) terraces, we demonstrate that Shockley electrons confined between a pair of isolated steps reveal negligible leakage ($T^2 < 0.1$ at $\sim E_F$), even in the presence of a continuum of states at the adjacent terrace.

ACKNOWLEDGMENTS

This work was supported in part by the Spanish MICINN (MAT2007-63083 and MAT2010-15659), the Basque Government (IT-257-07), and the Agència de Gestió d'Ajuts Universitaris i de Recerca (2009 SGR 695). The SRC is funded by the National Science Foundation (Award No. DMR-0084402). A.M. and J.L.-C. acknowledge funding from the Ramon y Cajal Fellowship program.

[1] M. F. Crommie, C. P. Lutz, and D. M. Eigler, Nature (London) **363**, 524 (1993).
[2] M. Crommie, J. Electron Spectrosc. Relat. Phenom. **109**, 1 (2000).
[3] J. Kliewer, R. Berndt, and S. Crampin, New J. Phys. **3**, 22 (2001).
[4] F. Klappenberger, D. Kühne, W. Krenner, I. Silanes, A. Arnau, F. J. García de Abajo, S. Klyatskaya, M. Ruben, and J. V. Barth, Phys. Rev. Lett. **106**, 026802 (2011).
[5] J. Lobo-Checa, M. Matena, K. Müller, J. H. Dil, F. Meier, L. H. Gade, T. A. Jung, and M. Stöhr, Science **325**, 300 (2009).
[6] J. Li, W.-D. Schneider, and R. Berndt, Phys. Rev. B **56**, 7656 (1997).
[7] L. Bürgi, O. Jeandupeux, H. Brune, and K. Kern, Phys. Rev. Lett. **82**, 4516 (1999).
[8] L. Bürgi, O. Jeandupeux, A. Hirstein, H. Brune, and K. Kern, Phys. Rev. Lett. **81**, 5370 (1998).
[9] C. Didiot, Y. Fagot-Revurat, S. Pons, B. Kierren, and D. Malterre, Surf. Sci. **601**, 4029 (2007).
[10] Z. Alpichshev, J. G. Analytis, J.-H. Chu, I. R. Fisher, Y. L. Chen, Z. X. Shen, A. Fang, and A. Kapitulnik, Phys. Rev. Lett. **104**, 016401 (2010).
[11] J. Seo, P. Roushan, H. Beidenkopf, Y. S. Hor, R. J. Cava, and A. Yazdani, Nature (London) **466**, 343 (2010).
[12] A. Mugarza and J. E. Ortega, J. Phys.: Condens. Matter **15**, S3281 (2003).
[13] F. Baumberger, M. Hengsberger, M. Muntwiler, M. Shi, J. Krempasky, L. Patthey, J. Osterwalder, and T. Greber, Phys. Rev. Lett. **92**, 016803 (2004).
[14] J. E. Ortega, M. Corso, Z. M. Abd-el Fattah, E. A. Goiri, and F. Schiller, Phys. Rev. B **83**, 085411 (2011).
[15] N. Zaki, K. Knox, P. D. Johnson, J. Fujii, I. Vobornik, G. Panaccione, and R. M. Osgood, Phys. Rev. B **83**, 205420 (2011).
[16] M. Hansmann, J. I. Pascual, G. Ceballos, H.-P. Rust, and K. Horn, Phys. Rev. B **67**, 121409 (2003).
[17] J. E. Ortega, S. Speller, A. R. Bachmann, A. Mascaraque, E. G. Michel, A. Närmann, A. Mugarza, A. Rubio, and F. J. Himpsel, Phys. Rev. Lett. **84**, 6110 (2000).
[18] P. Wahl, L. Diekhoner, M. A. Schneider, and K. Kern, Rev. Sci. Instrum. **79**, 043104 (2008).
[19] M. Corso, F. Schiller, L. Fernández, J. Cordón, and J. E. Ortega, J. Phys.: Condens. Matter **21**, 353001 (2009).

[20]M. Henzler, Appl. Phys. **9**, 11 (1976).

[21]A. Mugarza, A. Mascaraque, V. Repain, S. Rousset, K. N. Altmann, F. J. Himpsel, Y. M. Koroteev, E. V. Chulkov, F. J. García de Abajo, and J. E. Ortega, Phys. Rev. B **66**, 245419 (2002).

[22]P. Borghetti, J. Lobo-Checa, E. Goiri, A. Mugarza, F. Schiller, J. E. Ortega, and E. E. Krasovskii, J. Phys.: Condens. Matter **24**, 395006 (2012).

[23]For the red data we have applied a self-correction process for the surface orientation in order to achieve vertical $(2n + 1)\pi/2d$ rods. The output is the effective miscut angle, which is found to deviate less than 5% from the nominal value. A similar process applied to nanostripes demonstrated that ARPES is coherently restricted to local nanofacet planes [see J. Lobo-Checa *et al*., New J. Phys. **13**, 103013 (2011)].

[24]K. Morgenstern, K.-F. Braun, and K.-H. Rieder, Phys. Rev. Lett. **89**, 226801 (2002).

[25]T. Uchihashi, P. Mishra, K. Kobayashi, and T. Nakayama, Phys. Rev. B **84**, 195466 (2011).

[26]O. Jeandupeux, L. Bürgi, A. Hirstein, H. Brune, and K. Kern, Phys. Rev. B **59**, 15926 (1999).

[27]G. Nicolay, F. Reinert, S. Hüfner, and P. Blaha, Phys. Rev. B **65**, 033407 (2001).

[28]L. C. Davis, M. P. Everson, R. C. Jaklevic, and W. Shen, Phys. Rev. B **43**, 3821 (1991).